Magnetic resonance imaging manifestations of cerebral small vessel disease: automated quantification and clinical application

Lei Zhao[1], Allan Lee[1], Yu-Hua Fan[2], Vincent C.T. Mok[3,4], Lin Shi[5]

[1]BrainNow Research Institute, Shenzhen, Guangdong 518000, China;

[2]Department of Neurology, The First Affiliated Hospital, Sun Yat-sen University; Guangdong Provincial Key Laboratory for Diagnosis and Treatment of Major Neurological Diseases, National Key Clinical Department and Key Discipline of Neurology, Guangzhou, Guangdong 510080, China;

[3]Department of Medicine and Therapeutics, The Chinese University of Hong Kong, Hong Kong 999077, China;

[4]Gerald Choa Neuroscience Centre, Margaret KL Cheung Research Centre for Management of Parkinsonism, Therese Pei Fong Chow Research Centre for Prevention of Dementia, Lui Che Woo Institute of Innovative Medicine, The Chinese University of Hong Kong, Hong Kong 999077, China;

[5]Department of Imaging and Interventional Radiology, The Chinese University of Hong Kong, Hong Kong 999077, China.

Abstract

The common cerebral small vessel disease (CSVD) neuroimaging features visible on conventional structural magnetic resonance imaging include recent small subcortical infarcts, lacunes, white matter hyperintensities, perivascular spaces, microbleeds, and brain atrophy. The CSVD neuroimaging features have shared and distinct clinical consequences, and the automatic quantification methods for these features are increasingly used in research and clinical settings. This review article explores the recent progress in CSVD neuroimaging feature quantification and provides an overview of the clinical consequences of these CSVD features as well as the possibilities of using these features as endpoints in clinical trials. The added value of CSVD neuroimaging quantification is also discussed for researches focused on the mechanism of CSVD and the prognosis in subjects with CSVD.

Keywords: Cerebral small vessel disease; Neuroimaging manifestations; Automated quantification; Clinical relevance

Introduction

Cerebral small vessel disease (CSVD) is a disorder of cerebral microvessels that causes abnormalities visible on brain imaging. Neuroimaging features of CSVD include recent small subcortical infarct (RSSI), white matter (WM) hyperintensity, lacune, perivascular space (PVS), cerebral microbleed (CMB), and brain atrophy, according to the standards for reporting vascular changes on neuroimaging (STRIVE).[1] CSVD is a major contributor to vascular or mixed dementia and it causes at least 20% of all strokes worldwide.[1] CSVDs are also risk factors for a wide range of other neurological or psychiatric disorders. In this regard, increasing efforts have been made to automatically quantify the magnetic resonance imaging (MRI) manifestations of CSVD (samples of segmentation or detection are shown in Figure 1) for a better efficiency and reproducibility in research or clinical settings, and/or to associate these MRI features with possible clinical consequences for a better understanding of CSVD. In this review, we provided an overview of the progress in automatic quantification for neuroimaging features of CSVD and the clinical consequences of different MRI features of CSVD. In addition, we discussed the impact of neuroimaging quantification techniques on CSVD research and the need of well-established automatic quantification tools of CSVD imaging features for use in clinical practice. Of note, this review focused on the CSVD imaging features that are visible on conventional structural MRI as detailed in STRIVE criteria. Although, some CSVD features from advanced MRI modalities[2] (eg, diffusion tensor imaging) have been validated for their robustness for clinical studies[3,4] or even as secondary outcomes in clinical trials[5] (eg, peak width of skeletonized mean diffusivity that could sensitively capture CSVD progression), they would not be discussed in the following sections.

Automatic Quantification of MRI Features of CSVD

RSSI

Clinically evident RSSI, also known as lacunar stroke, refers to recent infarction (occurring in the previous few

Correspondence to: Lin Shi, Department of Imaging and Interventional Radiology, The Chinese University of Hong Kong, Hong Kong 999077, China
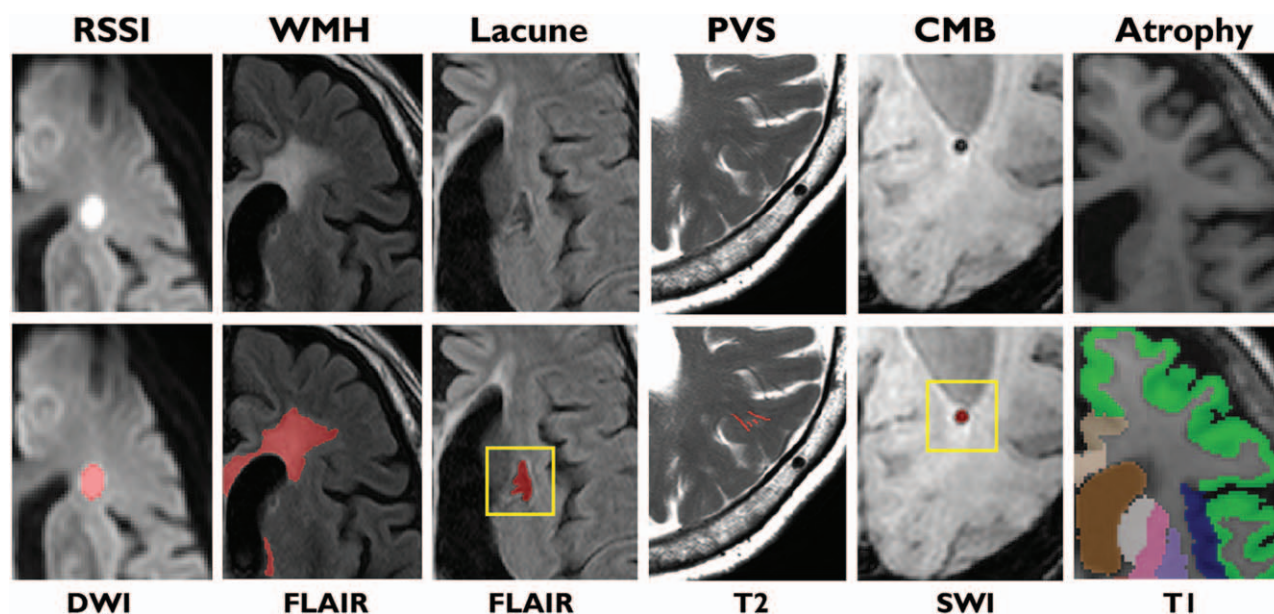E-Mail: shilin@cuhk.edu.hk

Figure 1: MRI manifestations of CSVD and the corresponding samples from segmentation or detection. The red masks indicate the segmentation results of the CSVD imaging features and the yellow rectangle points to the location of the CSVD feature for detection; the colored masks are obtained from the brain tissue and anatomical structure segmentation to measure the brain atrophy. The MRI sequences that help to visualize the CSVD imaging features are labeled at the bottom. CMB: Cerebral microbleed; CSVD: Cerebral small vessel disease; DWI: Diffusion-weighted imaging; MRI: Magnetic resonance imaging; RSSI: Recent small subcortical infarct; WMH: White matter hyperintensity; PVS: Perivascular space; FLAIR: Fluid-attenuated inversion recovery.

weeks) in the territory of one perforating artery, which causes about 25% of ischemic strokes.[1] RSSIs can be identified on MRI diffusion-weighted imaging (DWI) sequence as hyperintense lesions of up to 20 mm in diameter on axial sections. The quantification of RSSIs is generally based on visual check (for presence) or manual delineation (for volumetric evaluation) in clinical studies. The related automated quantification methods usually take acute ischemic lesions (including large acute infarcts) as a global category and do not limit to RSSIs for algorithm development. In fact, the accurate automatic segmentation of acute lesions on DWI is very challenging, due to the very low image resolution of DWI (as used in clinical practice), the presence of various mimics and high noise level in DWI scans, and the large variations in lesion size and location.[6] The early automated segmentation methods[7] for acute lesions on DWI generally utilized low-level features (eg, intensity and edge information) which are not robust enough to account for the large variations in lesion patterns. In contrast, the increasingly used deep learning methods in recent studies can extract high-level features of lesion patterns and have achieved better performance than the traditional methods. For example, with a large dataset of 242 acute ischemic stroke patients, Zhang et al[6] applied a deep convolutional neural networks (CNN) that extracts 3D contextual information and automatically learns discriminative features. This method achieved a Dice similarity coefficient (DSC, indicating spatial agreement of automatic segmentation results with the ground truth) of 79.13% and lesion-wise precision of 92.67%. Of note, the testing sample of this study contained about one-third of RSSIs among the acute infarcts, and thus this method should be applicable for the segmentation of RSSIs.

White matter hyperintensity (WMH)

WMHs are identifiable on fluid-attenuated inversion recovery (FLAIR) and T2-weighted (T2w) MRI as hyperintense lesions. The most widely used visual rating method of WMH is Fazekas' scale, where WMH is divided into periventricular WMH (PWMH) and deep WMH (DWMH) regarding the location, and each region is given a grade depending on the size and confluence of lesions.[8]

The automatic quantification methods of WMH can be classified into unsupervised and supervised methods. The unsupervised methods generally utilize the intensity features for clustering and do not need additional training, while the supervised methods may extract higher level information and rely on sufficient data of manual delineations as the ground truth for training. In general, the DSC of unsupervised methods was up to 0.899,[9] and for the supervised methods the DSC was up to 0.80.[10] In fact, the performances of different WMH segmentation methods are generally not fully comparable, due to the difference of subject characteristics and lesion load across studies. For example, the methods that achieved DSC of >0.80 were generally evaluated in stroke patients[11] or patients with vascular dementia,[9] where the patients tend to have larger lesion burden of WMH. Also, researchers found that the DSC of WMH segmentation increases with the lesion load, and a recent study reported the average DSC values of 0.51, 0.70, and 0.84 for low, medium, and high lesion load of WMH with the same segmentation method.[12] In this regard, independent evaluations for different level of lesion load should be encouraged for a better generalizability of the segmentation performance. Additionally, worldwide challenges provide fair opportunities for comparison of state-of-the-art WMH segmen-

tation methods. In the WMH segmentation challenge at MICCAI 2017, a large dataset of WMH ground truth was provided, and all the top ten participants applied deep learning methods[13] that have shown great potential in automated quantification of medical imaging. The winner of this challenge[10] used CNNs with ensemble models and achieved a DSC of 0.80. This method also showed good inter-scanner robustness and high efficiency (only 8 s needed per scan with a GPU of 12 GB RAM memory during testing), which are both important for practical applications.

Lacunes

Lacunes display as round or ovoid subcortical fluid-filled cavities in MRI with diameters of approximately 3 to 15 mm. Lacunes present as hypointensities in T1-weighted (T1w) and FLAIR images and hyperintensities in T2w images (approximate to the intensity of cerebrospinal fluid [CSF]).[1] Only a very few studies proposed automatic methods for lacune detection, and they generally used intensity-based algorithms. For example, Uchiyama *et al*[14] applied intensity-based region growing for candidate screening and used rule-based schemes and a support vector machine for the false-positive elimination, resulting in a sensitivity (SE) of 96.8% with 0.76 false positive (FP) per slice. In addition, Wang *et al*[15] applied a multi-stage segmentation scheme for WMH, cortical infarct, and lacunes, and achieved a SE of 83.3% with 0.06 FP per subject and a specificity of 96.6% for lacune detection. With the largest benchmark dataset available for lacune detection, Ghafoorian *et al*[16] proposed a two-stage method using deep CNN with information from both FLAIR and T1w images, and achieved a SE of 97.4% with 0.13 FP per slice.

CMBs

CMBs can be identified as small (up to 10 mm) areas of signal void on MRI sequences such as T2*-weighted gradient-recalled echo (GRE) or susceptibility-weighted images (SWI), and the SWI was reported to have better reliability and SE for CMB detection than T2*GRE.[17] In clinical routine, the annotation of CMBs is usually based on a visual inspection and manual localization.[18] However, there exist various types of CMB mimics (eg, flow voids, calcifications and cavernous malformations, iron deposition in the basal ganglia, and signal void due to poor flow compensation or cusp artifacts caused by failures in coil combination) which would resemble the appearance of CMBs in SWI scans. The manual inspection could suffer from limited reproducibility among different raters and could be time-consuming, laborious, and prone to errors, particularly for patients with large numbers of CMBs.

Alternatively, automatic detection methods can help alleviate the workload of neuroradiologists and improve the reliability and efficiency to identify CMB. In the early stage, automatic CMBs detection methods generally utilized morphological features based on shape, size, and intensity information, with the help of spherical descriptors, such as radial symmetry transform. Among these methods, Van den Heuvel *et al*[19] achieved the best performance with SE of 89% and FP per true CMB (FP/CMB) of 0.29. With the development of deep learning techniques, supervised CMB detection methods with CNN generally achieved better performance, as more powerful high-level features can be extracted by CNN for CMB detection. In a study with the largest benchmark dataset available for CMB detection on SWI, Dou *et al*[20] applied 3D CNN and achieved a SE of 93.16%, precision of 44.31%, and FP/CMB of 1.17. When using 7T SWI instead of 1.5T/3T SWI[21] or using phase image in addition to SWI,[22] slightly better SE (94.7%, 95.8%) and FP/CMB (0.37, 0.39) and much higher precision (71.9%, 70.9%) can be achieved. However, the poor accessibility of 7T MRI device and the availability of phase image should also be considered for application in clinical practice. Of note, the CMB detection per subject can be accomplished within 1 min with the CNN methods, thanks to the increasing computational power of GPU,[20] where the datasets for evaluation contain patients with large diversity in pathology and lesion burden (eg, stroke patients and normal elderly subjects).

PVS

PVS, also known as Virchow-Robin spaces, are fluid-filled spaces that follow the typical course of cerebral penetrating vessels and have a similar signal intensity with CSF on all MRI sequences (eg, hyperintense on T2w images). PVS are difficult for manual delineation due to their small size (with a diameter of <3 mm generally) and different appearance (linear or round) depending on the viewing plane.[1] Although PVS are commonly microscopic and not visible on conventional MRI, enlarged PVS (EPVS) become increasingly apparent as the patient age increases and are associated with other imaging manifestations of CSVD, such as WMHs and lacunes.[1,23,24] The most widely used visual rating scale of EPVS is Wardlaw scale[25] as rated on T2w image, which provides independent ratings for EPVS in midbrain, basal ganglia, and centrum semiovale.

Compared with WMH and CMB, the development of automatic quantification methods for EPVS falls much behind, probably due to the lack of accurate manual delineation masks of EPVS available for training. In this regard, some researchers turned to automatic qualitative rating of EPVS with visual rating of EPVS as the ground truth for algorithm training and evaluation. For example, Dubost *et al*[26] developed an automated rating method of EPVS based on 3D regression fully CNN on 1.5T T2w image and achieved an intraclass correlation coefficient (ICC) of 0.75 to 0.88, which was even higher than the inter-observer reliability from human raters. The only one study that used manually delineated PVS masks as the ground truth for learning was based on 7T MRI, where Park *et al*[27] applied Haar-like features (for object recognition) with random forest as the classifier and achieved a SE of 69% and a DSC of 0.73 for cluster-based segmentation accuracy. As 7T MRI has poor accessibility and 1.5T/3T MRI has relatively poor resolution for ground truth construction of EPVS, researchers proposed intensity-based semi-automatic EPVS segmentation method or tried to fit the segmentation algorithm with the visual

rating result as the reference for training. Wuerfel *et al*[28] applied a rater independent threshold-based semi-automatic post-processing routine and achieved an ICC of 0.996 in EPVS counts for intra-rater reliability. Ballerini *et al*[29] trained an ordered logit model to simulate the relationship between the number of PVS and the visual rating categories and achieved a Spearman correlation of 0.74 ($P < 0.001$) between the automated PVS count and the visual rating result.

Brain atrophy

Brain atrophy can be assessed in particular lobes, selective tissues, or specific brain regions. The available visual rating scales of atrophy generally focuses on lobar regions, such as Scheltens' scale of medial temporal atrophy, the frontal subscale of Pasquier's Global Cortical Atrophy scale, and Koedam's scale of Posterior Atrophy. A few studies attempted to implement these visual ratings automatically for a better reproducibility and efficiency.[30] More detailed assessment of regional brain atrophy generally relies on segmentation of brain tissues and specific structures, where manual delineation is more time-consuming than visual rating of lobar regions. In this regard, automatic segmentation methods have been developed and increasingly used in research and even clinical settings.

Automatic brain segmentation can be classified as tissue segmentation (ie, WM, gray matter [GM], and CSF) and anatomical structure segmentation (eg, supratentorial structures such as hippocampus, and infratentorial structures such as cerebellum or brainstem). The tissue segmentation methods can be subdivided into region-based, thresholding-based, clustering-based, and feature extraction and classification-based methods.[31] Statistical parametric mapping (SPM, a clustering-based software package) is one of the most commonly employed methods for automatic brain tissue segmentation, and it was reported to achieve an average voxel classification accuracy of 0.84 for GM and 0.87 for WM.[31] Classification-based methods, especially those with deep learning, generally performed the best for brain tissue segmentation, according to the worldwide challenges, such as MRBrainS13 and MRBrainS18. For example, the winner of MRBrainS13 used 3D deep learning (*voxnet1*) and achieved average DSC values of 0.86, 0.89, and 0.84 for GM, WM, and CSF, respectively.[32]

Regarding the anatomical structure segmentation, the methods include atlas-based (based on the accurate alignment of atlas priors), learning-based (based on an annotated training set), and algorithmic methods (relies on intensity information to a greater extent, eg, region-based and deformable methods). Different methods may have certain pros and cons for the segmentation of specific structures. For example, atlas-based approaches achieve good results when segmenting the hippocampus (DSC: 0.75–0.90), thalamus (DSC: 0.88–0.92), and lateral ventricle (DSC: 0.83–0.93), while deformable methods perform better for caudate (DSC: 0.84–0.91) and putamen (DSC: 0.86–0.89) in literature.[33] The increasingly used of deep learning-based segmentation methods seem to perform even better with an average DSC of 0.85 to

0.90 across all deep GM structures,[34] but comprehensive fair comparisons between these different methods are still lacking. In addition, the computational cost should never be ignored, as a combination of accuracy and efficiency for brain segmentation tools should be favorable for clinical use (eg, AccuBrain® outperforms FreeSurfer in both efficiency and accuracy in a study for hippocampus segmentation[35]). Also, the volume of some lesion features of CSVD (eg, lacune) in specific structures should not be excluded for brain structure segmentation,[36] and multi-atlas-based methods may perform better than algorithmic methods in this case.[37]

To sum up, as visual rating or manual delineation of the CSVD MRI features are time-consuming and subject to poor reproducibility, automatic quantification methods have been developed and increasingly used in research or clinical settings. The metrics of quantification performance for these CSVD features are different, which depend on the purpose of quantification (eg, detection or segmentation) and aspect of measurement (eg, spatial agreement or volumetric agreement). The deep learning methods have been increasingly used for the quantification of CSVD imaging features and generally present a better performance compared with the traditional methods. Nonetheless, worldwide challenges for fair comparisons of the quantification methods and lesion-burden-specific report of the performance are encouraged for generalizable applications in clinical studies. The general objective of quantification and the representative performance of the automatic methods for these CSVD imaging features were listed Table 1.

Clinical Relevance of MRI Features of CSVD

Clinical consequences

RSSI

RSSIs are symptomatic in most cases and they may not always evolve into lacunes but remain as mainly non-cavitated WMHs or even disappear after several weeks or months.[38] In 20% to 30% of patients with RSSIs, deterioration of neurological deficits occurs in hours or even days following the stroke onset.[39] The neurological dysfunctions after RSSIs may involve motor function or cognitive impairment, and the degree and domain of dysfunction largely depend on lesion location.[40] In patients with symptomatic RSSIs, the initial mortality and early stroke recurrence is low, and the recovery of deficits is generally good in the first few weeks after onset.[41]

WMH

Although the definitions of the boundary between PWMH and DWMH are generally not consistent, previous studies have consistently reported that PWMH and DWMH have different functional, microstructural, and clinical correlates.[42] WMHs are reported to be associated with impairment in global cognition and multiple cognitive domains (eg, executive functions and speed of mental

Table 1: Purpose of quantification and representative results of automatic quantification of CSVD imaging features.

| CSVD feature | Purpose of quantification | | Representative performance of automatic quantification[‡] | Computational cost[§] | |
	Segmentation	Detection		Time	Hardware
RSSI[*]	√		DSC = 0.79[6]	0.095 s per scan	GPU of 12 GB RAM
WMH	√		DSC = 0.80[10]	8 s per scan	GPU of 12 GB RAM
Lacune		√	SE = 97.4%, FP = 0.13 per slice[16]	NA	NA
CMB		√	SE = 95.8%, FP = 0.39 per CMB[21]	2 min per scan	GPU of 12 GB RAM
EPVS	√	√	DSC = 0.73[27]; r = 0.74[29]	NA	NA
Brain atrophy[†]	√		DSC = 0.85–0.90	NA	NA

[*]The presented method did not limit to the segmentation of RSSIs but also applied to other acute ischemic lesions. [†]Quantification of brain atrophy refers to brain segmentation of different structures and scales, and thus only a general range of DSC is provided. [‡]The representative performance not necessarily corresponds to the best performance, as a fair comparison of the studies is not possible due to the difference in patient characteristics or lesion burden. [§]The computational cost corresponds to the study that is listed for representative performance of automatic quantification, and the time displayed here only refers to the time needed for testing (training not considered). CSVD: Cerebral small vessel disease; RSSI: Recent small subcortical infarct; WMH: White matter hyperintensity; CMB: Cerebral microbleed; EPVS: Enlarged perivascular space; DSC: Dice similarity coefficient; SE: Sensitivity; FP: False positive; r: Spearman correlation coefficient; NA: Not available.

processing) in the population-based or memory clinic cohorts,[43] and there are some strategic locations (eg, anterior thalamic radiation and forceps minor) or specific shape descriptors (eg, shape irregularity) that trigger stronger associations than total WMH volume with the cognitive deficits.[44,45] WMHs also contribute to brain atrophy patterns in regions related to Alzheimer disease dementia, therefore, the strategies to prevent the development of WMHs may help to decrease the incidence of dementia or delay the onset of dementia.[46] In stroke patients, the lesion burden and locations of pre-existing WMHs are also independently related to post-stroke cognitive decline on top of infarcts.[47,48] Also, the WMH volume is associated with stroke recurrence after adjusting for clinical risk factors, and the association is stronger for hemorrhagic stroke than ischemic stroke.[49] In addition, WMHs may independently contribute to some other symptoms, such as post-stroke depression (PSD),[50] incident parkinsonism,[51] and sleep disorder.[52]

CMBs

In the community-based elderly cohort, the presence of lobar CMBs are associated with changes in cognitive function (especially in visuospatial executive functions),[53] and participants with any CMB had 1.74 times higher risk of dementia, whereas those with deep and mixed CMB had a threefold increased risk of dementia with a mean follow-up of 6.7 years.[54] Mixed (deep and lobar) or a higher load of CMBs (≥3), with some specificity for location, was associated with accelerated cognitive decline with a mean follow-up of 5.2 years in a population-based elderly cohort.[55] Also, the number of deep CMBs was associated with attention/executive dysfunction in non-dementia patients with CSVD.[56] Regarding the patients with stroke or transient ischemic attack (TIA), a high CMB number is weakly associated with executive dysfunction and the CMBs (especially in the deep regions) are associated with the dysfunction in attention domain.[57,58] In addition, first-episode mild ischemic stroke patients with three or more mixed CMBs had four times higher risk of developing post-stroke dementia in 2 years compared to patients with no CMBs.[59] In a study with pooled analysis of individual data from 20,322 patients with recent ischemic stroke or TIA (cumulative follow-up of 35,225 patient-years, median 1.34 years), CMBs are associated with a greater relative hazard for recurrent intracranial hemorrhage (ICH) than for ischemic stroke; the relative hazard ratio was positively associated with CMB burden for ICH, while this effect was less marked for ischemic stroke.[60] Of note, all these associations were independent from CMB anatomical distribution, antithrombotic treatment, ethnicity, age, and the presence of pre-existing WMHs.

Lacunes

The cause of most lacunes is presumed to be small subcortical infarcts, either symptomatic or silent.[1] Regarding the symptomatic lacunes (more often called lacunar infarcts), they generally refer to the chronic phase of RSSI and their functional consequences were generally not separated from those of silent lacunes in literatures. In fact, silent lacunes might differ from symptomatic infarcts only with respect to the lack of acute stroke-like signs, and they do present as subtle deficits in physical and cognitive function that commonly go unnoticed. For example, the presence of silent infarcts more than doubles the risk of subsequent stroke and dementia[61] and is associated with poor executive function (the association disappeared after additional adjustment for WMHs).[62] The total number of lacunar infarcts independently predicted incident vascular cognitive impairment among CSVD patients in 3 to 5 years.[63] Lacunar infarcts in the anteromedial thalamus are associated with impaired processing speed in CSVD patients.[64] Also, the locations of lacunar infarcts do matter for the associations with PSD, and the cumulative vascular burden resulting from chronic accumulation of lacunar infarcts within the thalamus, basal ganglia, and deep WM may be more important than single infarcts in the prediction of PSD.[65] In addition, a high number of lacunes is associated with incident parkinsonism.[51]

PVS

In a dementia-free population-based cohort, EPVS were associated with decline in information processing speed and more than quadrupled the risk of vascular dementia during a 5-year follow-up.[23] In a cross-sectional study also with dementia-free elderlies as the participants, the association of EPVS counts with cognitive dysfunction were not found;[66] however, another study that applied automatic EPVS segmentation[29] found that the volume of centrum semi-ovale EPVS (CSO-EPVS) was associated with memory adjusting for age, sex, vascular risk factors, childhood intelligence, and WMH.[67] The inconsistency might result from the better SE of computational metrics than visual rating in EPVS quantification.[24] Researchers also reported the association preference of CSO-EPVS with Alzheimer's disease and basal ganglia EPVS (BG-EPVS) with subcortical vascular cognitive impairment, indicating the potential of EPVS location to facilitate the differentiation of these two types of cognitive impairment.[68] Regarding the patients with stroke or TIA, BG-EPVS are independently associated with cognitive impairment at 1 year after stroke or TIA, even after adjusting for clinical confounders and other CSVD imaging features, such as WMH, lacune, and brain atrophy.[69] In addition, EPVS (either in centrum semi-ovale or basal ganglia) are associated with lower health-related quality of life in patients with mild to moderate acute ischemic stroke.[70] The association of CSO-EPVS with PSD was also found at 3 months after mild to moderate acute ischemic stroke, after adjusting for demographic, clinical, and imaging characteristics (including the number or presence of acute infarcts).[71] Moreover, a high number of BG-PVS was associated with increased risk of recurrent stroke (ischemic) in patients with ischemic stroke or TIA and incident stroke (ischemic or ICH) in community-dwelling individuals, while these associations were not reproduced for CS-PVS[72,73] Furthermore, EPVS may also contribute to cognitive decline in Parkinson's disease (PD) patients (BG-EPVS in particular)[74] and sleep disorders.[75]

Brain atrophy

Unlike the other CSVD image manifestations which are discrete focal lesions, the generalized brain atrophy is probably secondary to a diffuse process. The pathological changes of brain atrophy are heterogeneous and not necessarily indicative of neuronal loss.[1] Brain atrophy occurs not only in many disorders but also in normal ageing process, although the degree is different between healthy ageing and incident neurological disorders. Brain atrophy is associated with cognitive impairment and dementia, and regional atrophy (eg, hippocampal atrophy) has been used as a significant biomarker of neurodegeneration in early detection of Alzheimer disease.[76] In fact, global or regional brain atrophy is present in many neurological disorders (eg, multiple sclerosis,[77] PD,[78] and sleep disorder[79]) and psychiatric disorders (eg, post-traumatic stress disorder[80]). Brain atrophy is also associated with the presence of other types of CSVD imaging features (eg, WMH,[46] CMB,[81] lacune,[82] and EPVS[83]) and may have mediation effect on their functional consequences.

Possibility as endpoint in clinical trials

The most widely used CSVD MRI feature as one of the endpoints in clinical trials related to CSVD progression is WMH, followed by brain atrophy, and CMB or lacune. EPVS has not been even suggested for use in clinical trials, which may result from the lack of consistent findings in clinical consequence or the poor progress of development for robust quantification tools.[2] Among the CSVD imaging features discussed in this review, RSSI is the only lesion type of acute phase. The clinical trials that involve RSSI generally target the patients for prevention of possible recurrent stroke (ICH or ischemic stroke) and the outcome rarely constrains to recurrent RSSI.[84]

WMHs

The WMH volume has been increasingly used to evaluate subclinical cerebrovascular health,[85] and the progression of WMHs has been applied as a surrogate biomarker or outcome measure for the therapeutic or interventional trials in CSVD.[86,87]

Brain atrophy

The association between brain atrophy and worsening of cognitive function (eg, executive function[88]) has been established, and brain volume (eg, medial temporal lobe volume) has been used as a secondary outcome in a nutrition-related clinical trial among CSVD subjects.[89]

CMBs

Longitudinal changes of CMBs (ie, progression of CMBs) showed significant negative associations with executive function and global cognitive function in a memory clinic cohort, where the relations with cognitive performance were mainly driven by lobar CMBs, especially those located in temporal lobe.[90] The total number of new CMBs can be used to facilitate the evaluation of therapeutic efficacy for cerebral amyloid angiopathy (CAA) in a clinical trial.[87,91]

Lacunes

Lacunes may also fulfil the prerequisites of a surrogate marker (secondary surrogate endpoint in clinical trials), but the incidence of lacunes over short observational periods is small in the general population.[91] Despite of the fact, a clinical trial that aims to investigate the effect of low-dose statins to prevent the progression of CSVD in older hypertensive patients has applied new-incident lacunes as one of the endpoints.[87]

In summary, the CSVD imaging features have various clinical consequences and different extent of application in clinical trials as possible endpoints. Although automatic quantification methods of the CSVD imaging features have been developed, researchers still preferred visual rating or manual delineation for some CSVD imaging features (eg, lacune, CMB, and EPVS) in clinical studies. The representative clinical applications of CSVD MRI features were summarized in Table 2.

Table 2: Clinically relevant metrics, consequences, and the frequency of using automatic quantification in clinical studies for different CSVD imaging features.

CSVD features	Clinically relevant metrics	Representative clinical consequences		Clinical application of automatic quantification[†]	Used in clinical trials
		In stroke-free subjects	In stroke patients[*]		
RSSI	Volume and location	NA	Motor dysfunction and cognitive impairment	Rarely	NA
WMH	Volume, location, and shape	Cognitive impairment (dementia), PD, and sleep disorder	Cognitive decline, stroke recurrence, and depression	Frequently	Yes
CMB	Number and location	Cognitive impairment or decline (dementia)	Cognitive impairment (dementia), and stroke recurrence	Rarely	Yes
Lacune	Number and location	Stroke, cognitive impairment (dementia), and PD	Depression	Rarely	Yes
EPVS	Volume, number, width, and location	Cognitive impairment or decline (dementia), stroke, PD, and sleep disorder	Cognitive impairment, depression, quality of life, and stroke recurrence	Sometimes	NA
Brain atrophy	Volume and location	Cognitive impairment or decline (dementia)	NA	Frequently	Yes

[*]The displayed clinical consequences of a specific CSVD imaging feature (other than RSSI) in stroke patients indicate independent contribution to the outcomes on top of stroke lesions. [†]The frequency of using automatic quantification for each CSVD imaging feature in clinical studies is displayed. CSVD: Cerebral small vessel disease; RSSI: Recent small subcortical infarct; WMH: White matter hyperintensity; CMB: Cerebral microbleed; EPVS: Enlarged perivascular space; PD: Parkinson's disease; NA: Not available.

The Impact of Advanced Neuroimaging Quantification on CSVD

Better understanding of CSVD mechanism

With the development of neuroimaging techniques and the related automatic lesion quantification approaches, better understanding has been achieved about the relationships between different CSVD imaging manifestations and the underlying mechanisms of CSVD. For example, incident lacunes preferentially localizes to the edge of WMHs, suggesting that the mechanisms of lacunes and WMHs are intimately connected and that the edge of WMHs may serve as a predilection site for lacunes.[92] This finding is also in line with another study where both PWMH and DWMH were predictors for edge-localized infarction (RSSI).[93] In addition, one study with 7T MRI found a topographical association between a high degree of juxtacortical EPVS and cortical CMBs, supporting a common underlying pathophysiology (most likely CAA).[94] Furthermore, with the novel shape descriptors (elongation and planarity) of lacunes as automatically segmented with a seed-growing algorithm, researchers found that the main axis and plane of lacunes align with perforating arteries, which adds to current concepts on the mechanisms of lacunes.[95]

Better prognosis in subjects with CSVD

With the development of automatic quantification methods, more complex metrics of CSVD imaging features become available, especially for EPVS that have more morphological attributes (eg, length, width, sphericity, and orientation). A recent study that applied multidimensional computational metrics of EPVS found that these metrics increased the SE to detect associations of EPVS with risk exposures and neurological disease compared with simple count or visual score of EPVS.[24] In addition, the combination of different MRI manifestations of CSVD have been increasingly used for the prediction of cognitive and functional decline, as the different CSVD imaging features may have additive contributions to prognosis. The most widely used manner of "combination" is a total CSVD score, which generally depicts the presence or severity of each CSVD imaging feature based on visual rating and summarizes them as a composite score. However, the location of the CSVD neuroimaging features, which is also a key determinant of cognitive impairment,[96] cannot be captured in such a composite CSVD score. In a recent study that applied region of interest-based volumetric measurements of CSVD imaging features to predict post-stroke cognitive impairment (PSCI), an accuracy of >80% was achieved for the prediction of global cognition, where the burden of WMHs, lacunes, EPVS and brain atrophy in strategic regions jointly presented independent contribution to PSCI on top of acute ischemic lesions.[97]

These findings indicate that automatic quantification of volumetric and locational information of the CSVD imaging features may facilitate the prognosis in subjects with CSVD. To this end, the harmonization of quantification methods for CSVD imaging features should be essential to realize a generalizable translation for the prognosis in clinical practice.[2] In fact, there have been some automatic quantification tools of CSVD with validations in accuracy,

reproducibility, and efficiency, such as AccuBrain® that currently supports automatic quantification of brain atrophy[35,37] and WMH[98] and is promising for a more comprehensive quantification of CSVD features.

Conclusions

The robustness and efficiency of automatic quantification for CSVD imaging features have been greatly improved in the recent decade, especially with the aid of deep learning techniques. The CSVD imaging features are risk factors of various neurological and psychiatric disorders, and the automatic quantification of these features may better facilitate the prognosis in patients with CSVD than visual rating, as the automatic quantification provides more detailed volumetric and locational information and is more reproducible and efficient. In addition, the advanced neuroimaging quantification techniques could extract additional useful metrics of the CSVD imaging features (eg, shape descriptors of WMH and lacune) to facilitate researches especially in CSVD mechanism. Nonetheless, there is still a large gap between the established automatic quantification methods and the applications in clinical studies or practice, which primarily results from the lack of harmonization or the poor accessibility of these quantification techniques for general clinical researchers. To this end, well-validated and easy-to-use automatic tools that support robust quantifications of multiple CSVD imaging features should be favorable.

Conflicts of interest

L.S. is the director and V.M. is the medical advisor of BrainNow Medical Technology Limited. L.Z. and A.L. are now employed in BrainNow Medical Technology Limited. All other authors have no financial relationships with commercial interests.

References

1. Wardlaw JM, Smith EE, Biessels GJ, Cordonnier C, Fazekas F, Frayne R, et al. Neuroimaging standards for research into small vessel disease and its contribution to ageing and neurodegeneration. Lancet Neurol 2013;12:822–838. doi: 10.1016/s1474-4422(13)70124-8.
2. Smith EE, Biessels GJ, De Guio F, de Leeuw FE, Duchesne S, During M, et al. Harmonizing brain magnetic resonance imaging methods for vascular contributions to neurodegeneration. Alzheimers Dement (Amst) 2019;11:191–204. doi: 10.1016/j.dadm.2019.01.002.
3. Lam BYK, Leung KT, Yiu B, Zhao L, Biesbroek JM, Au L, et al. Peak width of skeletonized mean diffusivity and its association with age-related cognitive alterations and vascular risk factors. Alzheimers Dement (Amst) 2019;11:721–729. doi: 10.1016/j.dadm.2019.09.003.
4. Baykara E, Gesierich B, Adam R, Tuladhar AM, Biesbroek JM, Koek HL, et al. A novel imaging marker for small vessel disease based on skeletonization of white matter tracts and diffusion histograms. Ann Neurol 2016;80:581–592. doi: 10.1002/ana.24758.
5. Smith EE, Markus HS. New treatment approaches to modify the course of cerebral small vessel diseases. Stroke 2020;51:38–46. doi: 10.1161/STROKEAHA.119.024150.
6. Zhang R, Zhao L, Lou W, Abrigo JM, Mok VCT, Chu WCW, et al. Automatic segmentation of acute ischemic stroke from DWI using 3-D fully convolutional densenets. IEEE Trans Med Imaging 2018;37:2149–2160. doi: 10.1109/TMI.2018.2821244.
7. Prakash KNB, Gupta V, Bilello M, Beauchamp NJ, Nowinski WL. Identification, segmentation, and image property study of acute infarcts in diffusion-weighted images by using a probabilistic neural network and adaptive Gaussian mixture model. Acad Radiol 2006;13:1474–1484. doi: 10.1016/j.acra.2006.09.045.
8. Fazekas F, Chawluk JB, Alavi A, Hurtig HI, Zimmerman RA. MR signal abnormalities at 1.5 T in Alzheimer's dementia and normal aging. AJR Am J Roentgenol 1987;149:351–356. doi: 10.2214/ajr.149.2.351.
9. Jeon S, Yoon U, Park J-S, Seo SW, Kim J-H, Kim ST, et al. Fully automated pipeline for quantification and localization of white matter hyperintensity in brain magnetic resonance image. Int J Imaging Syst Technol 2011;21:193–200. doi: 10.1002/ima.20277.
10. Li H, Jiang G, Zhang J, Wang R, Wang Z, Zheng WS, et al. Fully convolutional network ensembles for white matter hyperintensities segmentation in MR images. Neuroimage 2018;183:650–665. doi: 10.1016/j.neuroimage.2018.07.005.
11. Shi L, Wang D, Liu S, Pu Y, Wang Y, Chu WC, et al. Automated quantification of white matter lesion in magnetic resonance imaging of patients with acute infarction. J Neurosci Methods 2013;213:138–146. doi: 10.1016/j.jneumeth.2012.12.014.
12. Simoes R, Monninghoff C, Dlugaj M, Weimar C, Wanke I, van Cappellen van Walsum AM, et al. Automatic segmentation of cerebral white matter hyperintensities using only 3D FLAIR images. Magn Reson Imaging 2013;31:1182–1189. doi: 10.1016/j.mri.2012.12.004.
13. Kuijf HJ, Biesbroek JM, De Bresser J, Heinen R, Andermatt S, Bento M, et al. Standardized assessment of automatic segmentation of white matter hyperintensities and results of the WMH segmentation challenge. IEEE Trans Med Imaging 2019;38:2556–2568. doi: 10.1109/TMI.2019.2905770.
14. Uchiyama Y, Yokoyama R, Ando H, Asano T, Kato H, Yamakawa H, et al. Computer-aided diagnosis scheme for detection of lacunar infarcts on MR images. Acad Radiol 2007;14:1554–1561. doi: 10.1016/j.acra.2007.09.012.
15. Wang Y, Catindig JA, Hilal S, Soon HW, Ting E, Wong TY, et al. Multi-stage segmentation of white matter hyperintensity, cortical and lacunar infarcts. Neuroimage 2012;60:2379–2388. doi: 10.1016/j.neuroimage.2012.02.034.
16. Ghafoorian M, Karssemeijer N, Heskes T, Bergkamp M, Wissink J, Obels J, et al. Deep multi-scale location-aware 3D convolutional neural networks for automated detection of lacunes of presumed vascular origin. Neuroimage Clin 2017;14:391–399. doi: 10.1016/j.nicl.2017.01.033.
17. Cheng AL, Batool S, McCreary CR, Lauzon ML, Frayne R, Goyal M, et al. Susceptibility-weighted imaging is more reliable than T2*-weighted gradient-recalled echo MRI for detecting microbleeds. Stroke 2013;44:2782–2786. doi: 10.1161/STROKEAHA.113.002267.
18. Gregoire SM, Chaudhary UJ, Brown MM, Yousry TA, Kallis C, Jager HR, et al. The microbleed anatomical rating scale (MARS): reliability of a tool to map brain microbleeds. Neurology 2009;73:1759–1766. doi: 10.1212/WNL.0b013e3181c34a7d.
19. van den Heuvel TL, van der Eerden AW, Manniesing R, Ghafoorian M, Tan T, Andriessen TM, et al. Automated detection of cerebral microbleeds in patients with traumatic brain injury. Neuroimage Clin 2016;12:241–251. doi: 10.1016/j.nicl.2016.07.002.
20. Dou Q, Chen H, Yu LQ, Zhao L, Qin J, Wang DF, et al. Automatic detection of cerebral microbleeds from MR images via 3D convolutional neural networks. IEEE Trans Med Imaging 2016;35:1182–1195. doi: 10.1109/Tmi.2016.2528129.
21. Chen Y, Villanueva-Meyer JE, Morrison MA, Lupo JM. Toward automatic detection of radiation-induced cerebral microbleeds using a 3D deep residual network. J Digit Imaging 2019;32:766–772. doi: 10.1007/s10278-018-0146-z.
22. Liu S, Utriainen D, Chai C, Chen Y, Wang L, Sethi SK, et al. Cerebral microbleed detection using susceptibility weighted imaging and deep learning. Neuroimage 2019;198:271–282. doi: 10.1016/j.neuroimage.2019.05.046.
23. Ding J, Sigurethsson S, Jonsson PV, Eiriksdottir G, Charidimou A, Lopez OL, et al. Large perivascular spaces visible on magnetic resonance imaging, cerebral small vessel disease progression, and risk of dementia: the age,

gene/environment susceptibility-Reykjavik study. JAMA Neurol 2017;74:1105–1112. doi: 10.1001/jamaneurol.2017.1397.

24. Ballerini L, Booth T, Valdes Hernandez MDC, Wiseman S, Lovreglio R, Munoz Maniega S, et al. Computational quantification of brain perivascular space morphologies: associations with vascular risk factors and white matter hyperintensities. A study in the Lothian Birth Cohort 1936. Neuroimage Clin 2020;25:102120. doi: 10.1016/j.nicl.2019.102120.

25. Potter GM, Chappell FM, Morris Z, Wardlaw JM. Cerebral perivascular spaces visible on magnetic resonance imaging: development of a qualitative rating scale and its observer reliability. Cerebrovasc Dis 2015;39:224–231. doi: 10.1159/000375153.

26. Dubost F, Yilmaz P, Adams H, Bortsova G, Ikram MA, Niessen W, et al. Enlarged perivascular spaces in brain MRI: automated quantification in four regions. Neuroimage 2019;185:534–544. doi: 10.1016/j.neuroimage.2018.10.026.

27. Park SH, Zong X, Gao Y, Lin W, Shen D. Segmentation of perivascular spaces in 7T MR image using auto-context model with orientation-normalized features. Neuroimage 2016;134:223–235. doi: 10.1016/j.neuroimage.2016.03.076.

28. Wuerfel J, Haertle M, Waiczies H, Tysiak E, Bechmann I, Wernecke KD, et al. Perivascular spaces - MRI marker of inflammatory activity in the brain? Brain 2008;131:2332–2340. doi: 10.1093/brain/awn171.

29. Ballerini L, Lovreglio R, Valdes Hernandez MDC, Ramirez J, MacIntosh BJ, Black SE, et al. Perivascular spaces segmentation in brain MRI using optimal 3D filtering. Sci Rep 2018;8:2132. doi: 10.1038/s41598-018-19781-5.

30. Martensson G, Ferreira D, Cavallin L, Muehlboeck JS, Wahlund LO, Wang C, et al. AVRA: automatic visual ratings of atrophy from MRI images using recurrent convolutional neural networks. Neuroimage Clin 2019;23:101872. doi: 10.1016/j.nicl.2019.101872.

31. Dora L, Agrawal S, Panda R, Abraham A. State-of-the-art methods for brain tissue segmentation: a review. IEEE Rev Biomed Eng 2017;10:235–249. doi: 10.1109/RBME.2017.2715350.

32. Chen H, Dou Q, Yu L, Qin J, Heng PA. VoxResNet: deep voxelwise residual networks for brain segmentation from 3D MR images. Neuroimage 2018;170:446–455. doi: 10.1016/j.neuroimage.2017.04.041.

33. Gonzalez-Villa S, Oliver A, Valverde S, Wang L, Zwiggelaar R, Llado X. A review on brain structures segmentation in magnetic resonance imaging. Artif Intell Med 2016;73:45–69. doi: 10.1016/j.artmed.2016.09.001.

34. Pagnozzi AM, Fripp J, Rose SE. Quantifying deep grey matter atrophy using automated segmentation approaches: a systematic review of structural MRI studies. Neuroimage 2019;201:116018. doi: 10.1016/j.neuroimage.2019.116018.

35. Abrigo J, Shi L, Luo Y, Chen Q, Chu WCW, Mok VCT, et al. Standardization of hippocampus volumetry using automated brain structure volumetry tool for an initial Alzheimer's disease imaging biomarker. Acta Radiol 2019;60:769–776. doi: 10.1177/0284185118795327.

36. De Guio F, Duering M, Fazekas F, De Leeuw FE, Greenberg SM, Pantoni L, et al. Brain atrophy in cerebral small vessel diseases: extent, consequences, technical limitations and perspectives: the HARNESS initiative. J Cereb Blood Flow Metab 2020;40:231–245. doi: 10.1177/0271678X19888967.

37. Wang C, Zhao L, Luo Y, Liu J, Miao P, Wei S, et al. Structural covariance in subcortical stroke patients measured by automated MRI-based volumetry. Neuroimage Clin 2019;22:101682. doi: 10.1016/j.nicl.2019.101682.

38. Pinter D, Gattringer T, Enzinger C, Seifert-Held T, Kneihsl M, Fandler S, et al. Longitudinal MRI dynamics of recent small subcortical infarcts and possible predictors. J Cereb Blood Flow Metab 2019;39:1669–1677. doi: 10.1177/0271678X18775215.

39. Del Bene A, Palumbo V, Lamassa M, Saia V, Piccardi B, Inzitari D. Progressive lacunar stroke: review of mechanisms, prognostic features, and putative treatments. Int J Stroke 2012;7:321–329. doi: 10.1111/j.1747-4949.2012.00789.x.

40. Zhao L, Biesbroek JM, Shi L, Liu W, Kuijf HJ, Chu WW, et al. Strategic infarct location for post-stroke cognitive impairment: a multivariate lesion-symptom mapping study. J Cereb Blood Flow Metab 2017;38:1299–1311. doi: 10.1177/0271678X17728162.

41. Arboix A, Marti-Vilalta JL. Lacunar stroke. Expert Rev Neurother 2009;9:179–196. doi: 10.1586/14737175.9.2.179.

42. Griffanti L, Jenkinson M, Suri S, Zsoldos E, Mahmood A, Filippini N, et al. Classification and characterization of periventricular and deep white matter hyperintensities on MRI: a study in older adults. Neuroimage 2018;170:174–181. doi: 10.1016/j.neuroimage.2017.03.024.

43. Kloppenborg RP, Nederkoorn PJ, Geerlings MI, van den Berg E. Presence and progression of white matter hyperintensities and cognition: a meta-analysis. Neurology 2014;82:2127–2138. doi: 10.1212/WNL.0000000000000505.

44. Biesbroek JM, Weaver NA, Hilal S, Kuijf HJ, Ikram MK, Xu X, et al. Impact of strategically located white matter hyperintensities on cognition in memory clinic patients with small vessel disease. PLoS One 2016;11:e0166261. doi: 10.1371/journal.pone.0166261.

45. Lange C, Suppa P, Maurer A, Ritter K, Pietrzyk U, Steinhagen-Thiessen E, et al. Mental speed is associated with the shape irregularity of white matter MRI hyperintensity load. Brain Imaging Behav 2017;11:1720–1730. doi: 10.1007/s11682-016-9647-x.

46. Habes M, Erus G, Toledo JB, Zhang T, Bryan N, Launer LJ, et al. White matter hyperintensities and imaging patterns of brain ageing in the general population. Brain 2016;139:1164–1179. doi: 10.1093/brain/aww008.

47. Jokinen H, Kalska H, Mantyla R, Ylikoski R, Hietanen M, Pohjasvaara T, et al. White matter hyperintensities as a predictor of neuropsychological deficits post-stroke. J Neurol Neurosurg Psychiatry 2005;76:1229–1233. doi: 10.1136/jnnp.2004.055657.

48. Zhao L, Wong A, Luo Y, Liu W, Chu WWC, Abrigo JM, et al. The additional contribution of white matter hyperintensity location to post-stroke cognitive impairment: insights from a multiple-lesion symptom mapping study. Front Neurosci 2018;12:290. doi: 10.3389/fnins.2018.00290.

49. Ryu WS, Schellingerhout D, Hong KS, Jeong SW, Jang MU, Park MS, et al. White matter hyperintensity load on stroke recurrence and mortality at 1 year after ischemic stroke. Neurology 2019;93:e578–e589. doi: 10.1212/WNL.0000000000007896.

50. O'Brien JT, Firbank MJ, Krishnan MS, van Straaten EC, van der Flier WM, Petrovic K, et al. White matter hyperintensities rather than lacunar infarcts are associated with depressive symptoms in older people: the LADIS study. Am J Geriatr Psychiatry 2006;14:834–841. doi: 10.1097/01.JGP.0000214558.63358.94.

51. van der Holst HM, van Uden IW, Tuladhar AM, de Laat KF, van Norden AG, Norris DG, et al. Cerebral small vessel disease and incident Parkinsonism: the RUN DMC study. Neurology 2015;85:1569–1577. doi: 10.1212/WNL.0000000000002082.

52. Thurston RC, Wu M, Aizenstein HJ, Chang Y, Mitchell EB, Derby CA, et al. Sleep characteristics and white matter hyperintensities among midlife women. Sleep 2020;43:zsz298. doi: 10.1093/sleep/zsz298.

53. Chung CP, Chou KH, Chen WT, Liu LK, Lee WJ, Chen LK, et al. Strictly lobar cerebral microbleeds are associated with cognitive impairment. Stroke 2016;47:2497–2502. doi: 10.1161/STROKEAHA.116.014166.

54. Romero JR, Beiser A, Himali JJ, Shoamanesh A, DeCarli C, Seshadri S. Cerebral microbleeds and risk of incident dementia: the Framingham Heart Study. Neurobiol Aging 2017;54:94–99. doi: 10.1016/j.neurobiolaging.2017.02.018.

55. Ding J, Sigurethsson S, Jonsson PV, Eiriksdottir G, Meirelles O, Kjartansson O, et al. Space and location of cerebral microbleeds, cognitive decline, and dementia in the community. Neurology 2017;88:2089–2097. doi: 10.1212/WNL.0000000000003983.

56. Cao WW, Wang Y, Dong Q, Chen X, Li YS, Zhou Y, et al. Deep microbleeds and periventricular white matter disintegrity are independent predictors of attention/executive dysfunction in non-dementia patients with small vessel disease. Int Psychogeriatr 2017;29:793–803. doi: 10.1017/S1041610216002118.

57. Patel B, Lawrence AJ, Chung AW, Rich P, Mackinnon AD, Morris RG, et al. Cerebral microbleeds and cognition in patients with symptomatic small vessel disease. Stroke 2013;44:356–361. doi: 10.1161/STROKEAHA.112.670216.

58. Wang Z, Wong A, Liu W, Yang J, Chu WC, Au L, et al. Cerebral microbleeds and cognitive function in ischemic stroke or transient ischemic attack patients. Dement Geriatr Cogn Disord 2015;40:130–136. doi: 10.1159/000379744.

59. Yatawara C, Guevarra AC, Ng KP, Chander R, Lam BYK, Wong A, et al. The role of cerebral microbleeds in the incidence of post-stroke dementia. J Neurol Sci 2020;412:116736. doi: 10.1016/j.jns.2020.116736.

60. Wilson D, Ambler G, Lee K-J, Lim J-S, Shiozawa M, Koga M, et al. Cerebral microbleeds and stroke risk after ischaemic stroke or transient ischaemic attack: a pooled analysis of individual patient data from cohort studies. Lancet Neurol 2019;18:653–665. doi: 10.1016/s1474-4422(19)30197-8.

61. Vermeer SE, Longstreth WT Jr, Koudstaal PJ. Silent brain infarcts: a systematic review. Lancet Neurol 2007;6:611–619. doi: 10.1016/S1474-4422(07)70170-9.

62. Zhang M, Xie B, Gao J, Mak HKF, Kwong ASK, Chan DCP, et al. Distinct profiles of cognitive impairment associated with different silent cerebrovascular lesions in hypertensive elderly Chinese. J Neurol Sci 2019;403:139–145. doi: 10.1016/j.jns.2019.06.028.

63. Pavlovic AM, Pekmezovic T, Tomic G, Trajkovic JZ, Sternic N. Baseline predictors of cognitive decline in patients with cerebral small vessel disease. J Alzheimers Dis 2014;42 (Suppl 3):S37–S43. doi: 10.3233/JAD-132606.

64. Benjamin P, Lawrence AJ, Lambert C, Patel B, Chung AW, MacKinnon AD, et al. Strategic lacunes and their relationship to cognitive impairment in cerebral small vessel disease. Neuroimage Clin 2014;4:828–837. doi: 10.1016/j.nicl.2014.05.009.

65. Santos M, Gold G, Kovari E, Herrmann FR, Bozikas VP, Bouras C, et al. Differential impact of lacunes and microvascular lesions on poststroke depression. Stroke 2009;40:3557–3562. doi: 10.1161/STROKEAHA.109.548545.

66. Hilal S, Tan CS, Adams HHH, Habes M, Mok V, Venketasubramanian N, et al. Enlarged perivascular spaces and cognition: a meta-analysis of 5 population-based studies. Neurology 2018;91:e832–e842. doi: 10.1212/WNL.0000000000006079.

67. Valdes Hernandez MDC, Ballerini L, Glatz A, Munoz Maniega S, Gow AJ, Bastin ME, et al. Perivascular spaces in the centrum semiovale at the beginning of the 8th decade of life: effect on cognition and associations with mineral deposition. Brain Imaging Behav 2019;14:1865–1875. doi: 10.1007/s11682-019-00128-1.

68. Banerjee G, Kim HJ, Fox Z, Jager HR, Wilson D, Charidimou A, et al. MRI-visible perivascular space location is associated with Alzheimer's disease independently of amyloid burden. Brain 2017;140:1107–1116. doi: 10.1093/brain/awx003.

69. Arba F, Quinn TJ, Hankey GJ, Lees KR, Wardlaw JM, Ali M, et al. Enlarged perivascular spaces and cognitive impairment after stroke and transient ischemic attack. Int J Stroke 2018;13:47–56. doi: 10.1177/1747493016666091.

70. Liang Y, Deng M, Chen YK, Mok V, Wang DF, Ungvari GS, et al. Enlarged perivascular spaces are associated with health-related quality of life in patients with acute ischemic stroke. CNS Neurosci Ther 2017;23:973–979. doi: 10.1111/cns.12766.

71. Liang Y, Chan YL, Deng M, Chen YK, Mok V, Wang F, et al. Enlarged perivascular spaces in the centrum semiovale are associated with poststroke depression: a 3-month prospective study. J Affect Disord 2018;228:166–172. doi: 10.1016/j.jad.2017.11.080.

72. Lau KK, Li L, Lovelock CE, Zamboni G, Chan TT, Chiang MF, et al. Clinical correlates, ethnic differences, and prognostic implications of perivascular spaces in transient ischemic attack and ischemic stroke. Stroke 2017;48:1470–1477. doi: 10.1161/STROKEAHA.117.016694.

73. Duperron MG, Tzourio C, Schilling S, Zhu YC, Soumare A, Mazoyer B, et al. High dilated perivascular space burden: a new MRI marker for risk of intracerebral hemorrhage. Neurobiol Aging 2019;84:158–165. doi: 10.1016/j.neurobiolaging.2019.08.031.

74. Park YW, Shin NY, Chung SJ, Kim J, Lim SM, Lee PH, et al. Magnetic resonance imaging-visible perivascular spaces in basal ganglia predict cognitive decline in Parkinson's disease. Mov Disord 2019;34:1672–1679. doi: 10.1002/mds.27798.

75. Huang S, Wang D, Zhou H, Chen Z, Wang H, Li Y, et al. Neuroimaging consequences of cerebral small vessel disease in patients with obstructive sleep apnea-hypopnea syndrome. Brain Behav 2019;9:e01364. doi: 10.1002/brb3.1364.

76. Jack CR Jr, Bennett DA, Blennow K, Carrillo MC, Feldman HH, Frisoni GB, et al. A/T/N: an unbiased descriptive classification scheme for Alzheimer disease biomarkers. Neurology 2016;87:539–547. doi: 10.1212/WNL.0000000000002923.

77. Charil A, Yousry TA, Rovaris M, Barkhof F, De Stefano N, Fazekas F, et al. MRI and the diagnosis of multiple sclerosis: expanding the concept of "no better explanation". Lancet Neurol 2006;5:841–852. doi: 10.1016/s1474-4422(06)70572-5.

78. Politis M. Neuroimaging in Parkinson disease: from research setting to clinical practice. Nat Rev Neurol 2014;10:708–722. doi: 10.1038/nrneurol.2014.205.

79. Kumar R, Farahvar S, Ogren JA, Macey PM, Thompson PM, Woo MA, et al. Brain putamen volume changes in newly-diagnosed patients with obstructive sleep apnea. Neuroimage Clin 2014;4:383–391. doi: 10.1016/j.nicl.2014.01.009.

80. Villarreal G, Hamilton DA, Petropoulos H, Driscoll I, Rowland LM, Griego JA, et al. Reduced hippocampal volume and total white matter volume in posttraumatic stress disorder. Biol Psychiatry 2002; 52:119–125. doi: 10.1016/s0006-3223(02)01359-8.

81. Chowdhury MH, Nagai A, Bokura H, Nakamura E, Kobayashi S, Yamaguchi S. Age-related changes in white matter lesions, hippocampal atrophy, and cerebral microbleeds in healthy subjects without major cerebrovascular risk factors. J Stroke Cerebrovasc Dis 2011;20:302–309. doi: 10.1016/j.jstrokecerebrovasdis.2009.12.010.

82. Appelman AP, Vincken KL, van der Graaf Y, Vlek AL, Witkamp TD, Mali WP, et al. White matter lesions and lacunar infarcts are independently and differently associated with brain atrophy: the SMART-MR study. Cerebrovasc Dis 2010;29:28–35. doi: 10.1159/000255971.

83. Zhang X, Ding L, Yang L, Qin W, Yuan J, Li S, et al. Brain atrophy correlates with severe enlarged perivascular spaces in basal ganglia among Lacunar stroke patients. PLoS One 2016;11:e0149593. doi: 10.1371/journal.pone.0149593.

84. Tsai HH, Kim JS, Jouvent E, Gurol ME. Updates on prevention of hemorrhagic and lacunar strokes. J Stroke 2018;20:167–179. doi: 10.5853/jos.2018.00787.

85. Ward SA, Raniga P, Ferris NJ, Woods RL, Storey E, Bailey MJ, et al. ASPREE-NEURO study protocol: a randomized controlled trial to determine the effect of low-dose aspirin on cerebral microbleeds, white matter hyperintensities, cognition, and stroke in the healthy elderly. Int J Stroke 2017;12:108–113. doi: 10.1177/1747493016669848.

86. Schmidt R, Berghold A, Jokinen H, Gouw AA, van der Flier WM, Barkhof F, et al. White matter lesion progression in LADIS: frequency, clinical effects, and sample size calculations. Stroke 2012;43:2643–2647. doi: 10.1161/STROKEAHA.112.662593.

87. Ji T, Zhao Y, Wang J, Cui Y, Duan D, Chai Q, et al. Effect of low-dose statins and apolipoprotein E genotype on cerebral small vessel disease in older hypertensive patients: a subgroup analysis of a randomized clinical trial. J Am Med Dir Assoc 2018;19:995–1002. e4. doi: 10.1016/j.jamda.2018.05.025.

88. Nitkunan A, Lanfranconi S, Charlton RA, Barrick TR, Markus HS. Brain atrophy and cerebral small vessel disease: a prospective follow-up study. Stroke 2011;42:133–138. doi: 10.1161/STROKEAHA.110.594267.

89. Bowman GL, Silbert LC, Dodge HH, Lahna D, Hagen K, Murchison CF, et al. Randomized trial of marine n-3 polyunsaturated fatty acids for the prevention of cerebral small vessel disease and inflammation in aging (PUFA trial): rationale, design and baseline results. Nutrients 2019;11:735. doi: 10.3390/nu11040735.

90. Li L, Wu DH, Li HQ, Tan L, Xu W, Dong Q, et al. Association of cerebral microbleeds with cognitive decline: a longitudinal study. J Alzheimers Dis 2020;75:571–579. doi: 10.3233/JAD-191257.

91. Schmidt R, Seiler S, Loitfelder M. Longitudinal change of small-vessel disease-related brain abnormalities. J Cereb Blood Flow Metab 2016;36:26–39. doi: 10.1038/jcbfm.2015.72.

92. Duering M, Csanadi E, Gesierich B, Jouvent E, Herve D, Seiler S, et al. Incident lacunes preferentially localize to the edge of white matter hyperintensities: insights into the pathophysiology of cerebral small vessel disease. Brain 2013;136:2717–2726. doi: 10.1093/brain/awt184.

93. Zhang X, Ding L, Yuan J, Qin W, Hu W. Spatial relationship between acute lacunar infarction and white matter hyperintensities. Eur Neurol 2015;74:259–266. doi: 10.1159/000442465.

94. Bouvy WH, van Veluw SJ, Kuijf HJ, Zwanenburg JJ, Kappelle JL, Luijten PR, et al. Microbleeds colocalize with enlarged juxtacortical perivascular spaces in amnestic mild cognitive impairment and early Alzheimer's disease: a 7 Tesla MRI study. J Cereb Blood Flow Metab 2020;40:739–746. doi: 10.1177/0271678X19838087.

95. Gesierich B, Duchesnay E, Jouvent E, Chabriat H, Schmidt R, Mangin JF, et al. Features and determinants of lacune shape: relationship with fiber tracts and perforating arteries. Stroke 2016;47:1258–1264. doi: 10.1161/STROKEAHA.116.012779.

96. Biesbroek JM, Weaver NA, Biessels GJ. Lesion location and cognitive impact of cerebral small vessel disease. Clin Sci 2017;131:715–728. doi: 10.1042/CS20160452.

97. Shi L, Zhao L, Yeung FK, Wong SY, Chan RKT, Tse MF, et al. Mapping the contribution and strategic distribution patterns of neuroimaging features of small vessel disease in poststroke cognitive impairment. J Neurol Neurosurg Psychiatry 2018;89:918–926. doi: 10.1136/jnnp-2017-317817.

98. Guo C, Niu K, Luo Y, Shi L, Wang Z, Zhao M, et al. Intra-scanner and inter-scanner reproducibility of automatic white matter hyperintensities quantification. Front Neurosci 2019;13:679. doi: 10.3389/fnins.2019.00679.